Supplementary Materials for:

A universal pathway for kinesin stepping

Bason E. Clancy[1], William M. Behnke-Parks[2], Johan O. L. Andreasson[3], Steven S. Rosenfeld[4], & Steven M. Block[1,5]

[1]Department of Biology, Stanford University, Stanford, CA 94305, USA.
[2]Department of Biology, Columbia University, New York, NY 10032, USA.
[3]Department of Physics, Stanford University, Stanford, CA 94305, USA.
[4]Department of Neurology, Columbia University, New York, NY 10032, USA.
[5]Department of Applied Physics, Stanford University, Stanford, CA 94305 USA.
Correspondence should be addressed to S.M.B. (sblock@stanford.edu).

Supplementary Figures

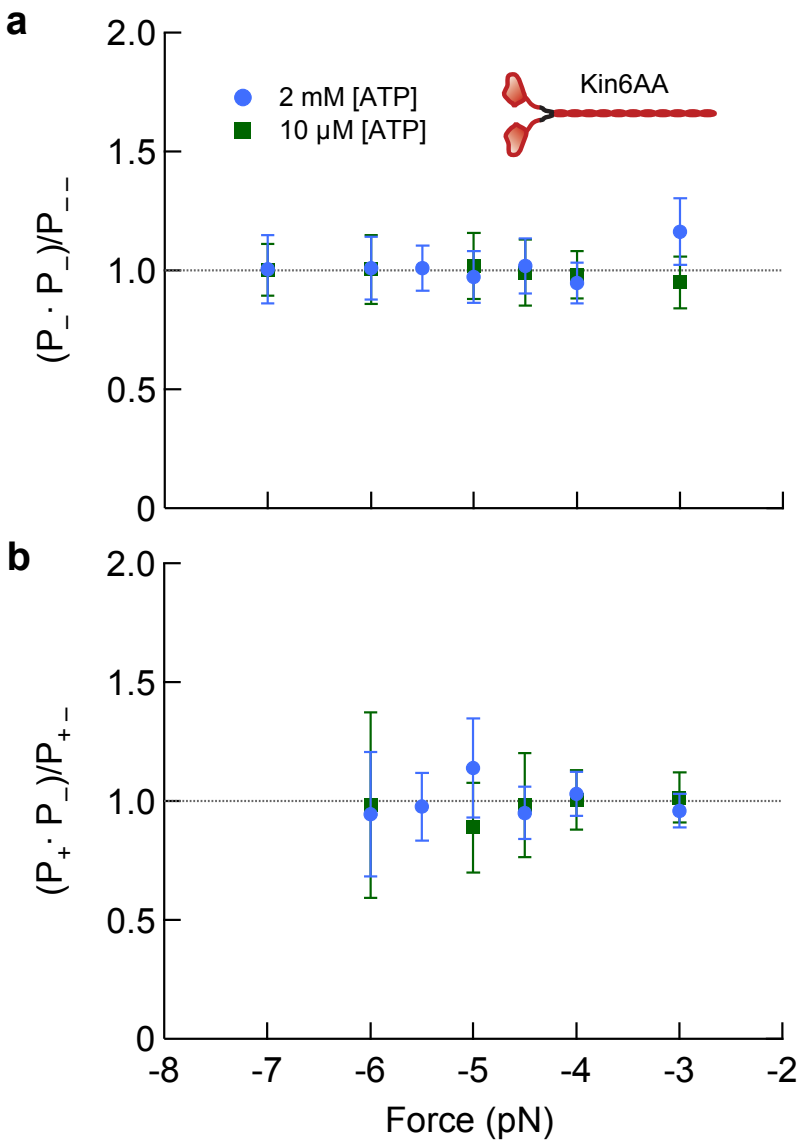

Figure 1 Lack of memory for successive steps. The estimated probabilities for taking a forward step or a backward step are given by $P_+ = n_+/(n_+ + n_-)$ and $P_- = n_-/(n_+ + n_-)$, where n_+ and n_- are the numbers of positive and negative steps scored at any given force and ATP concentration, respectively. The probability of observing two backward steps in succession will be given by $P_{- -} = n_{- -}/(n_{+ +} + n_{- -} + n_{+ -} + n_{- +})$, where the n_{ij} represent the numbers of pairs of successive forward steps $(++)$, pairs of successive backward steps $(- -)$, or pairs consisting of a step in each direction $(+ -, - +)$. From these expressions, it follows that $P_{+ -} = n_{+ -}/(n_{+ +} + n_{- -} + n_{+ -} + n_{- +})$. (**a**) The ratio of $(P_-)^2$ to $P_{- -}$ as a function of load. When successive steps are uncorrelated (zero memory), this ratio will tend to unity, since $P_{- -}$ will simply equal the probability of taking a single backward step, P_-, times the probability of taking another, statistically independent backward step, P_-. The experimentally determined ratio is statistically consistent with unity for all forces and ATP concentrations, demonstrating that steps have no memory of the preceding step direction (Markov property). (**b**) Analogous reasoning applies to the forward steps. The ratio of $(P_+ \cdot P_-)$ to $P_{+ -}$ as a function of load. As in (**a**), the ratio is unity for uncorrelated steps.

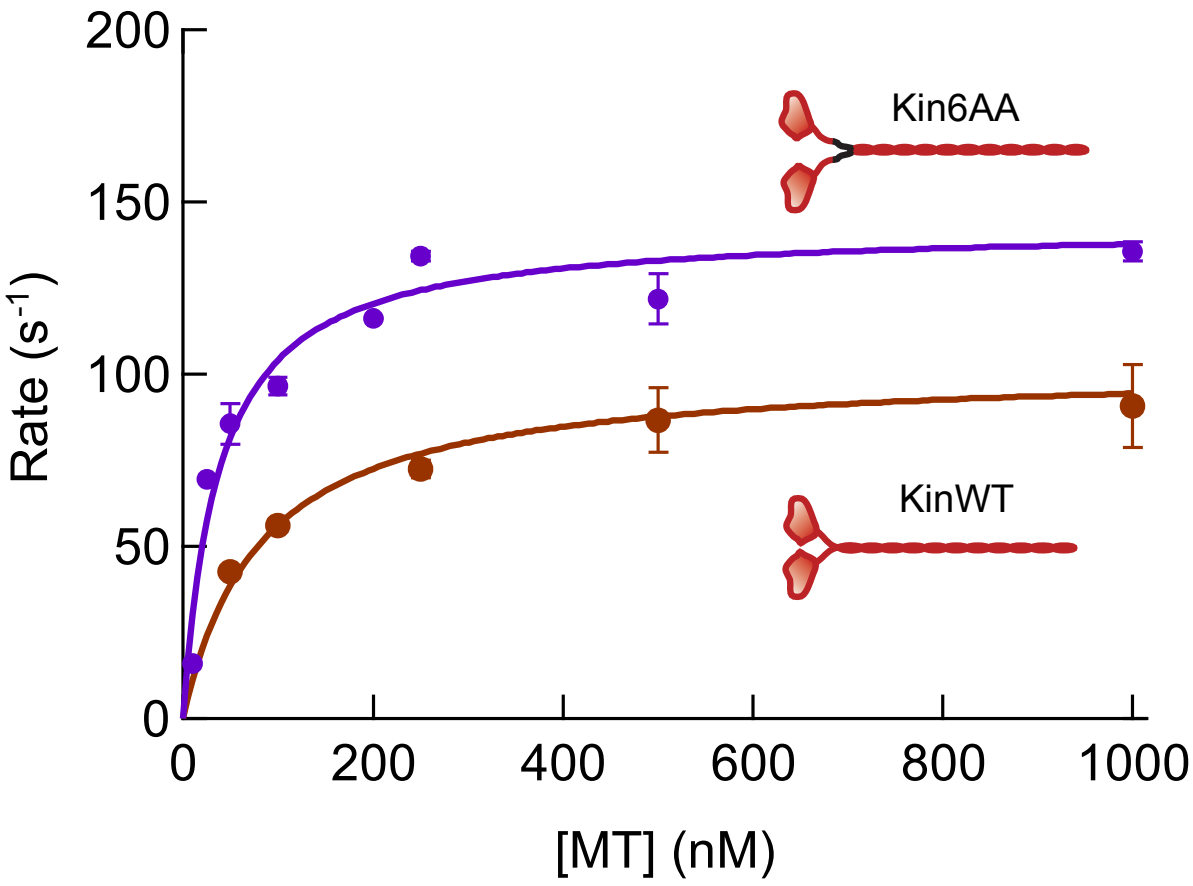

Figure 2 The ATPase rate per dimer for KinWT and Kin6AA. The plot shows the MT-stimulated ATPase rates for KinWT (red filled circles; mean ± s.e.m.; N = 3) and Kin6AA (purple filled circles; mean ± s.e.m.; N = 3) as a function of the MT concentration. The solid lines represent fits to the standard Michaelis-Menten expression. KinWT has an ATPase rate of 102 ± 4 s^{-1} per dimer and a $K_{0.5,\ MT}$ of 82 ± 14 nM. This is in contrast to Kin6AA, which has an ATPase rate of 143 ± 6 s^{-1} per dimer and a $K_{0.5,\ MT}$ of 38 ± 8 nM, roughly half that of KinWT. Under unloaded conditions, the average velocity of KinWT is 762 ± 7 nm s^{-1}; Kin6AA is slower, averaging 323 ± 4 nm s^{-1}. Assuming an 8 nm step size, these velocities imply head-stepping rates of 95 s^{-1} and 40 s^{-1} for KinWT and Kin6AA, respectively. The very similar values for ATP-hydrolysis and mechanical-stepping rates for KinWT (102 s^{-1}, 95 s^{-1}) imply that ATP hydrolysis is coupled 1:1 to motion. However, for Kin6AA (143 s^{-1}, 40 s^{-1}) the rate of ATP hydrolysis is significantly greater than the head-stepping rate, suggesting that, on average, multiple ATP molecules are hydrolyzed per 8-nm advance by this motor. This inefficiency is likely to be a consequence of futile hydrolysis, although some backstepping may contribute.

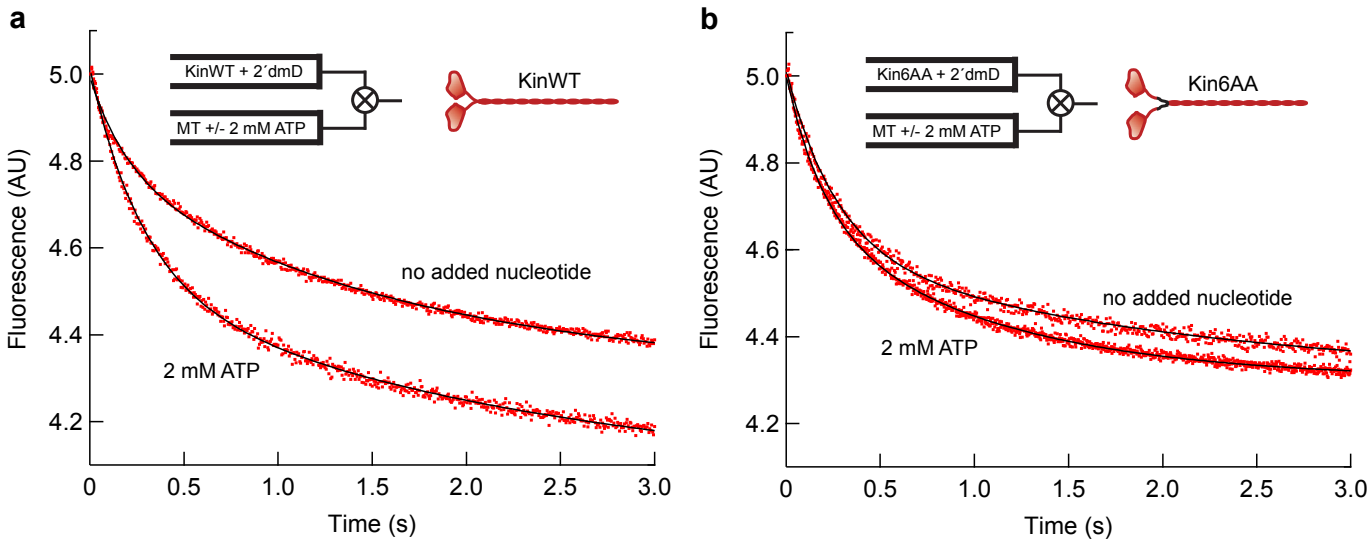

Figure 3 2′dmD release from KinWT and Kin6AA in the presence of microtubules. (**a**) The rate of 2′dmD release was measured by rapidly mixing KinWT (pre-incubated with equimolar amounts of 2′dmD) with MTs and 2 mM ATP, or MTs without ATP. When KinWT is mixed with MT without added nucleotide, the fluorescence amplitude is 66% of the amplitude in the presence of MTs and 2 mM ATP. (**b**) When the same experiment is performed with Kin6AA, mixing the motor with MTs without added nucleotide results in a fluorescence amplitude change that is 99% of the amplitude change experienced with the addition of 2 mM ATP.

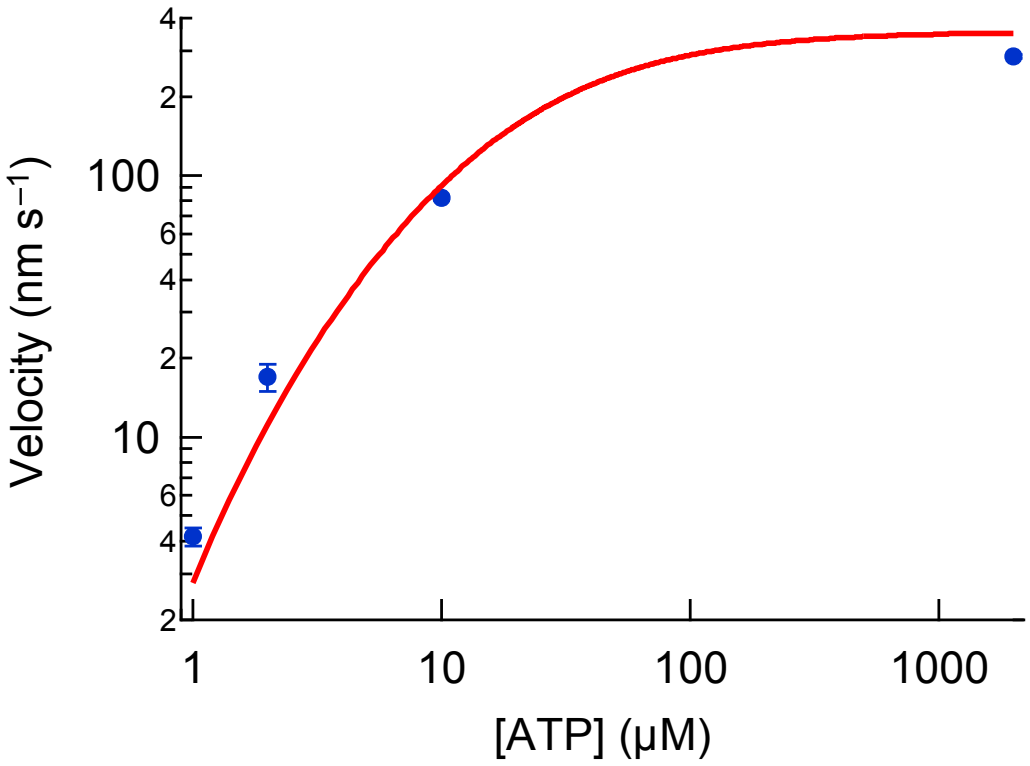

Figure 4 An independent test of the five-state model. The graph shows the unloaded velocity of forward stepping for Kin6AA as a function of ATP concentration. The experimental data (blue filled circles; mean ± s.e.m.; N = 8–179) are displayed together with the prediction of the five-state model (red solid line) using the rate constants of Table 1. The forward velocity values represent an independent dataset, because these were not used as a part of the global data for the model fit that generated the rate constants of Table 1. There are therefore no adjustable parameters involved in modeling the data shown here.

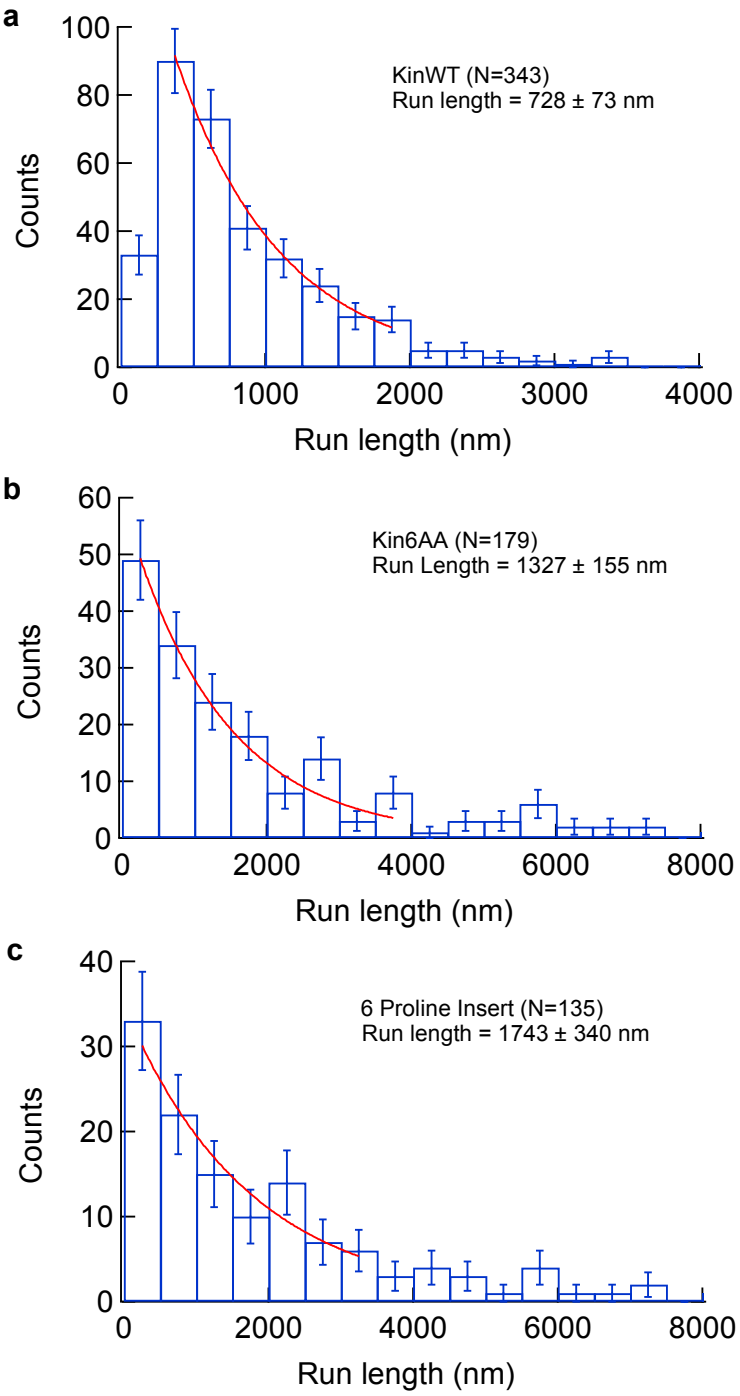

Figure 5 Processivities of KinWT, Kin6AA, and Kin6P. Run-length distributions were acquired under unloaded (F = 0) and saturating ATP (2 mM) conditions. Histograms are displayed with std. statistical errors and fits to an exponential, $A \cdot \exp(-x/x_0)$ (red lines); bins with <6 counts were not included in fits. (**a**) Distribution of run lengths for KinWT. The characteristic run length estimate, based on fit parameter x_0, is 728 ± 73 nm. (**b**) Distribution of run lengths for Kin6AA. The characteristic run length estimate is 1,327 ± 155 nm. (**c**) Distribution of run lengths for Kin6P. The characteristic run length estimate is 1,743 ± 340 nm. All three constructs were found to be fully processive; the processivities of Kin6AA and Kin6P were comparable and somewhat longer than for KinWT.

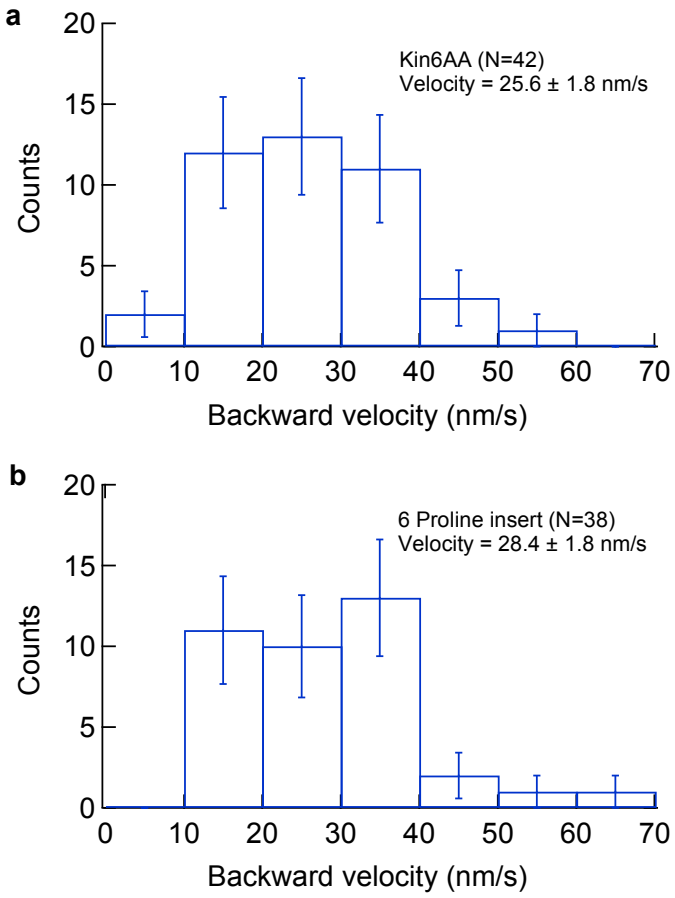

Figure 6 Average backward velocities under load for the Kin6AA and Kin6P constructs carrying neck-linker inserts. The KinWT linker insert sequence is AEQKLT; the Kin6P (6-proline) insert is KKPPPPPPG. Data were acquired under−7 pN hindering load and 2 mM ATP. (**a**) Histogram of velocities for Kin6AA, with associated errors. The mean velocity for the distribution is 25.6 ± 1.8 nm/s (mean ± s.e.m.) Velocities were computed from the slopes of linefits to single-molecule records of position vs. time. (**b**) Histogram of velocities for Kin6P. The mean velocity for the distribution is 28.4 ± 1.8 nm/s (mean ± s.e.m.) The Kin6AA and Kin6P velocities are statistically indistinguishable, within error.

Supplementary Methods

Single-molecule experiments

Global curve fitting. The single-molecule data in **Figs. 1** and **2** (main text) were fit using the mechano-chemical model presented in **Fig. 3** (main text). Global fits of the M = 10 model parameters (and associated parameter errors) of **Table 1** to the N = 73 data points displayed in **Figs. 1** and **2**, corresponding to $N–M$ = 63 degrees of freedom, were carried out using software written in Igor (Wavemetrics, Inc.) that implements the Levenberg-Marquardt algorithm for minimization. Reaction diagrams composed of states connected by rate constants, of the type displayed in **Fig. 3**, are generally modeled by systems of coupled, first-order differential equations. Such systems can represented by a single Master Equation, with vectors that correspond to the arrays of input and output states connected by a matrix comprised of the transition rates. The eigenvalues of the transition matrix, for example, supply the time constants for relaxation of the system. However, unless the transition matrix happens to be sparse, it is not generally possible to solve analytically for the eigenvalues and eigenvectors of any matrices larger than 4 x 4. However, as Chemla *et. al*[1] have shown using Fourier-Laplace transform techniques, expressions for the velocity and randomness of any reaction system can be obtained analytically, in closed form, directly from the three lowest order terms of the characteristic equation of the transition matrix, without any need to solve for its eigenvalues or eigenvectors. Analytical expressions for the velocity (v), step ratio (SR) and randomness (r) were obtained by applying their published formalism to the reaction system in **Fig. 3** with the aid of Mathematica (Wolfram Research, Inc.). These expressions are:

$$v = v_+ - v_- = (\gamma'_+ - \gamma'_-)/\beta$$

step ratio, $SR = \gamma'_+/\gamma'_-$

$$r = (\gamma''/\gamma' + 2\,\beta'/\beta - 2\,\alpha\,\gamma'/\beta^2)\cdot d^{-1}$$

where d is the step size and

$$\gamma'_+ = d \cdot [\mathrm{ATP}]^2 \cdot k_{23} \cdot k_{31} \cdot k_{12} \cdot (k_{51} \cdot k_{45} + k_{51} \cdot k_{43} + k_{54} \cdot k_{43})$$

$$\gamma'_- = d \cdot [\mathrm{ATP}] \cdot [k_{14} \cdot k_{51} \cdot k_{45} \cdot (k_{31} + k_{34}) \cdot (k_{23} + k_{25} + k_{21}) + [\mathrm{ATP}] \cdot k_{25} \cdot k_{51} \cdot k_{12} \cdot (k_{31} \cdot k_{45} + k_{31} \cdot k_{43} + k_{45} \cdot k_{34})]$$

$$\gamma' = \gamma'_+ - \gamma'_-$$

$$\gamma'' = d \cdot (\gamma'_+ + \gamma'_-)$$

$$\beta = k_{14} \cdot (k_{51} + k_{54}) \cdot (k_{31} + k_{34}) \cdot (k_{23} + k_{25} + k_{21}) + [\mathrm{ATP}] \cdot \big[k_{45} \cdot (k_{14} + k_{51}) \cdot (k_{31} + k_{34}) \cdot (k_{23} + k_{25} + k_{21}) + k_{43} \cdot (k_{14} + k_{31}) \cdot (k_{51} + k_{54}) \cdot (k_{23} + k_{25} + k_{21}) + k_{12} \cdot \big(k_{25} \cdot k_{54} \cdot (k_{31} + k_{34}) + k_{23} \cdot k_{34} \cdot (k_{51} + k_{54})\big)\big] + [\mathrm{ATP}]^2 \cdot k_{12} \cdot [k_{45} \cdot (k_{25} + k_{51}) \cdot (k_{31} + k_{34}) + k_{45} \cdot k_{23} \cdot (k_{51} + k_{34}) + k_{43} \cdot (k_{23} + k_{31}) \cdot (k_{51} + k_{54}) + k_{43} \cdot k_{25} \cdot (k_{31} + k_{54})]$$

$$\beta' = d \cdot [\mathrm{ATP}] \cdot [k_{23} \cdot k_{31} \cdot k_{12} \cdot (k_{54} + k_{51}) - k_{25} \cdot k_{51} \cdot k_{12} \cdot (k_{31} + k_{34}) - k_{14} \cdot k_{51} \cdot k_{45} \cdot (k_{23} + k_{25} + k_{21} + k_{31} + k_{34})] + d \cdot [\mathrm{ATP}]^2 \cdot k_{12} \cdot (k_{45} + k_{43}) \cdot (k_{23} \cdot k_{31} - k_{25} \cdot k_{51})$$

$$\alpha = (k_{23} + k_{25} + k_{21} + k_{14}) \cdot (k_{54} + k_{51}) \cdot (k_{34} + k_{31}) + k_{14} \cdot (k_{51} + k_{54} + k_{31} + k_{34}) \cdot (k_{23} + k_{25} + k_{21}) + [\mathrm{ATP}] \cdot [k_{12} \cdot k_{23} \cdot (k_{51} + k_{34}) + k_{12} \cdot k_{54} \cdot (k_{23} + k_{25}) + k_{12} \cdot (k_{51} + k_{54} + k_{25}) \cdot (k_{34} + k_{31}) + k_{45} \cdot (k_{51} + k_{14} + k_{31} + k_{34}) \cdot (k_{23} + k_{25} + k_{21}) + k_{45} \cdot (k_{51} + k_{14}) \cdot (k_{31} + k_{34}) + k_{43} \cdot (k_{51} + k_{54} + k_{31} + k_{14}) \cdot (k_{23} + k_{25} + k_{21}) + k_{43} \cdot (k_{31} + k_{14}) \cdot (k_{51} + k_{54})] + [\mathrm{ATP}]^2 \cdot k_{12} \cdot [k_{45} \cdot (k_{23} + k_{25} + k_{51} + k_{31} + k_{34}) + k_{43} \cdot (k_{23} + k_{25} + k_{31} + k_{51} + k_{54})]$$

[ATP] is the ATP concentration and the k_{ij} are the rates between states. The minus sign was swapped between the second and third terms in the expression for r, above, to account for any change of sign in the velocity (i.e., forward or backstepping). Load dependence was introduced by multiplying k_{23}, k_{25}, and k_{14} by the appropriate Boltzmann factor, $\exp(F \cdot \delta_{ij} / k_B T)$, where F is the force, δ_{ij} is a characteristic distance, and $k_B T$ is the thermal energy. The resulting equations for v, SR, and r are explicit functions of the parameters, k_{ij} and δ_{ij}, and the ATP concentration. We note that they are not functions of the ADP or P_i concentrations, which are taken to be negligible in the domain of applicability of this model.

All transitions involving the binding of ATP to the kinesin head were taken to proceed at rates proportional to the ATP concentration, and therefore modeled by (pseudo) second-order binding constants (k_{12}, k_{43}, k_{45}). This approximation is valid over the range of loads and concentrations studied here. In actuality, such rates will saturate at the highest ATP levels in a Michaelis-Menten-type fashion, because the formation of a weak collision complex between ATP and the motor domain is followed by a transition to a tighter binding state that takes finite time. If K_D represents the dissociation constant for the ATP-head collision complex, then

$$k = \frac{k_{\max}[\mathrm{ATP}]}{[\mathrm{ATP}] + K_D}$$

describes the saturation of these binding rates (derived below). Based on the data for **Figure 5b**, we obtain K_D = 632 ± 270 μM and k_{max} = 1,517 ± 443 s^{-1} for the binding of the analog 2′dmT, which likely represents a lower bound for ATP itself. At 2 mM ATP, these values imply a binding rate in excess of 1,153 ± 337 s^{-1}. That rate is to be compared with the next-fastest rate returned by our fitting, which is the load-dependent stepping transition, $k_{23} = k_{23}^0 \exp[F\delta/k_B T]$. From the data in **Table 1**, the value for the step transition at −1 pN load (i.e., the worst-case scenario) is (570 s^{-1})exp(−4.3/4.05) = 197 s^{-1}, which is already nearly six-fold slower than the ATP binding rate. For all other loads studied (−2 pN on up), the stepping transition slows to 68 s^{-1} or below, which becomes comparable to other reaction rates (e.g., to the ATP dissociation rate from the front head), all of which are more than an order of magnitude slower than the saturated ATP binding rate. ATP binding is therefore well approximated by a second-order binding constant, with a rate proportional to the ATP concentration.

Ensemble fluorescence experiments

Derivation of dissociation rate constant for ATP release from ensemble kinetic measurements. As previously demonstrated[2], we can depict the reaction of 2′dmT with a microtubule-kinesin complex as follows:

$$M \cdot K + T \overset{K_D}{\leftrightarrow} M \cdot K \cdot T \overset{k_1/k_{-1}}{\longleftrightarrow} M \cdot K \cdot T^* \overset{k_2/k_{-2}}{\longleftrightarrow} M \cdot K \cdot D^* \cdot P_i \overset{k_3}{\rightarrow} M \cdot K \cdot D^*$$

where M is the microtubule, K is kinesin, T is 2′dmT, D is 2′dmD, and P_i is inorganic phosphate. The binding of 2′dmT first occurs via the formation of a collision complex (characterized by the dissociation constant K_D) followed by a first-order transition that produces enhancement of the 2′dmT fluorescence (designated by an asterisk, with associated rate constants k_1 and k_{-1}). The hydrolysis of ATP (k_2/k_{-2}) is followed by phosphate release (k_3), which under the conditions of the experiment is essentially irreversible. The solution of the rate equations for each state has been described previously[3-5]. At low [2′dmT], the observed rate constant is c/b, where:

$$b = \bar{k}_1 + k_{-1} + k_2 + k_{-2} + k_3 \ ,$$

$$c = \bar{k}_1(k_2 + k_{-2} + k_3) + k_{-1}(k_{-2} + k_3) + k_2 k_3 \ \text{, and}$$

$$\bar{k}_1 = \frac{k_1 \cdot [T]}{[T] + K_D}$$

The *y*-intercept of the plot of the observed rate constant versus 2′dmT concentration (**Fig. 5b**, 61 ± 12 s^{-1}) defines an apparent dissociation rate constant, k_d, which can be derived by setting [T] to 0 in the ratio c/b:

$$k_d = \frac{(k_2 k_3 + k_{-1}(k_{-2} + k_3))}{(k_{-1} + k_2 + k_{-2} + k_3)}$$

Previous studies of the kinetics of ATP interaction with kinesin provide estimates for the values of k_2 (100-120 s^{-1}; refs. 2, 6) and k_3 (80-100 s^{-1}, ref. 7). Although the hydrolysis step (k_2/k_{-2}) is reversible in the presence of microtubules under certain conditions[8], $k_{-2} << k_2$ or k_3 and can therefore be ignored in the denominator. Using these values, we can derive a range of values of k_{-1}, the rate constant for ATP dissociation, from 55-135 s^{-1} (**Table 1**).

Methods for Figure 5, main text. The complex of 2.0 μM Kin6AA and 10 μM polymerized tubulin was made nucleotide-free by first incubating with apyrase (0.2 U ml^{-1}) and then mixing in the stopped-flow spectrometer with 40 μM 2′dmT. Conditions: 100 mM KCl, 25 mM HEPES, 2 mM $MgCl_2$, pH 7.50, 20°C.

ATPase activity. The MT-activated ATPase activities of KinWT and Kin6AA were measured in 25 mM HEPES (pH 7.5), 2 mM $MgCl_2$, 1 mM EGTA, 2 mM DTT, 20 mM KCl at 20°C with microtubules in a >50-fold molar excess over kinesin active site. The reaction was initiated by adding ATP to 2 mM, and was monitored using an EnzCheck Phosphate Assay Kit (Invitrogen).

Mutant construction. DNA for the kinesin mutants was generated by PCR from the KinWT construct in two fragments, and ligated into pET21 vector in a three-way ligation. All mutants utilized the same 5′ primer for the final PCR product,

CACACAGAATTCATGGCGGACCTGGGCGAG TCT AAT,

with the 3′ primer

CACACACTCGAGTTTTAGTAAAGATGCCATCTCAGCTGCTCG.

For both amino acid insert chimeras, the PstI site was used for digestion. For the 6 proline insert[9], the 5′ primer was

CACACACTGCAGTTCCTGGTGGTGGTGGTGGTGGCTTCTTTAACTCGCAATTGACACTAACTGTGTTCTTAATTG

with the 3′ primer

CACACA CTGCAG AAC AGT GGA AAA AGA AGT ATG AAA AAG AAA AAG AAA AAA ATA AGA TC.

For the six amino-acid insert, the sequence AEQKLT was introduced, and the identical 5′ primer for the proline insert was used, but changing the 3′ primer to

CACACA CTGC AGT TCC TGG TGG TGG TGG TGG TGG CTTCTT
ATATATAAATTTTTTTTCCCCTAACTCGCAATTGACACTAACTGTGTTCTTAATTG.

PCR products were digested with PstI and either XhoI or EcoRI, and ligated into pET21a plasmids for expression in BL21 cells. DNA for all constructs made was confirmed by sequencing.

Supplementary References

1. Chemla, Y.R., Moffitt, J.R. & Bustamante, C. Exact solutions for kinetic models of macromolecular dynamics. *J Phys Chem B* **112**, 6025-44 (2008).
2. Ma, Y.Z. and Taylor, E.W. Kinetic mechanism of microtubule kinesin ATPase. *Biochemistry*, **34**, 13242-13251 (1995).
3. Benson, S.W. *The Foundation of Chemical Kinetics.* R.E. Krieger Publishing Co., 1982; pp 36-40.
4. Trybus, K.M. and Taylor, E.W. Transient kinetic of adenosine 5'-diphosphate and adenosine 5' (β,γ-imidotriphosphate) binding to subfragment 1 and actosubfragment 1. *Biochemistry,* **21**, 1284-1294 (1982).
5. Hannemann, D.E. et al. Magnesium, ADP, and actin binding linkage of myosin V: evidence for multiple myosin V-ADP and actomyosin V-ADP states. *Biochemistry*, **44,** 8826-8840 (2005).
6. Gilbert, S.P. and Johnson, K.A. Pre-steady state kinetics of the microtubule-kinesin ATPase. *Biochemistry*, **33**, 1951-1960 (1994).
7. Moyer, M.L., Gilbert, S.P., and Johnson, K.A. Pathway of ATP hydrolysis by monomeric and dimeric kinesin. *Biochemistry*, **37** (3), 800–813 (1998).
8. Hackney, D.D. The tethered motor domain of a kinesin-microtubule complex catalyzes reversible synthesis of bound ATP. *Proc. Nat. Acad. Sci. USA*, **102**, 18338-18343 (2005).
9. Yildiz, A., Tomishige, M., Gennerich, A. & Vale, R.D. Intramolecular strain coordinates kinesin stepping behavior along microtubules. *Cell* **134**, 1030-41 (2008).